Progress In Electromagnetics Research, Vol. 120, 423–437, 2011

STUDIES OF POWER-COMBINING OF OPEN SLOT ANTENNA ARRAYS

C.-J. Wang and Y. Dai*

Department of Electrical Engineering, National University of Tainan, Tainan 700, Taiwan

Abstract—In this paper, we propose several array topologies to achieve good power-combining characteristics for the open slot antenna. By utilizing an appropriate feeding structure and injecting in-phase or out-of-phase signals, power-combining radiation patterns can be derived. Simulated surface current distributions of several antenna structures are presented to explain radiation mechanism. From the results of radiation performance, the advantages of gain enhancement and pattern reconfiguration are shown. By varying the phase difference of two injected signals of the open slot antenna array, two-dimensional beam-scanning radiation patterns are successfully demonstrated.

1. INTRODUCTION

Generally speaking, by arranging several antennas in space and interconnecting to produce a directional radiation pattern, such a configuration of multiple radiating elements is referred to as an antenna array. An array offers the important advantages of high antenna gain, narrow beam width, low side lobe, and electronically scanning beam [1]. In [2], the analysis is shown that for identical elements separated by an integral number of half wavelengths, stability can be predicted, with no additional information required, such that the good mutual coupling effect can be derived. Many past researches have been proposed for discussions and improvement of the power combining characteristics [3–7]. For example, in [3], an antenna array with lower sidelobes was demonstrated by utilizing a 16-element linear array. The factors affecting the sidelobe characteristics of the array were examined. In 1993, York proposed a new technique for phase-shifterless beam-scanning by using couple-oscillator array. By tuning

Received 15 August 2011, Accepted 23 September 2011, Scheduled 27 September 2011
* Corresponding author: Yang Dai (yangdai1027@gmail.com).

the frequencies of the end oscillators in the chain, the main beam could be steered over a range of angle 37°. A unilateral injection-locking active antenna array with electronic scanning performance was proposed in [5]. With a frequency tuning range of 30 MHz, the measured scanning range was 21°, approximately. The cost of the scanning antenna array could be reduced.

Recently, the open slot (or calling monopole slot) antenna attracts much attention due to its compact size for a fixed operating frequency. A quarter-wavelength open slot cut in the finite ground plane and fed by a microstrip transmission line, a wide impedance bandwidth and bi-directional radiation are provided [8–17]. It is different from the conventional shorted slot antenna resonating at a half-wavelength. Hence, the monopole slot antenna can occupies some value spaces on the system circuit board. Due to the monopole topology [8], co-polarized radiation patterns of the monopole slot antenna at different frequencies look omni-directional. Several different slot shapes were introduced to generate additional resonances so that bandwidth enhancement was achieved [9]. Furthermore, the occupied area of the antenna was decreased. In [10], a pentagon-shape slot was etched as a radiator on the ground plane, and a feeding line with a pentagon stub was used. This antenna demonstrates a superior ultra-wideband (UWB) impedance bandwidth. In [11], a simple folded slot was etched as a radiator on the ground plane, and a feeding line with a connecting strip was used. This antenna covers penta bands of WWAN operation and is suitable to be placed at the hinge of the clamshell mobile phone. Due to the radiation from a notch embedded in the ground plane, for the open slot antenna, the beams in the broadside cut planes are quasi-omnidirectional and the beamwidths are wide. A switched-beam antenna array has been demonstrated in [12]. The proposed antenna is mainly composed of a four-element array with radiation elements based on the L-shaped monopole slot antenna. By controlling four pin diodes of a single-pole-four-throw (SP4T) switch, switched-beam radiation patterns for WLAN applications are obtained in one plane. However, the main beam of the beam-switched antenna array can not continuously scan in the free space. Moreover, the beam shape is fan-like and the beamwidth seems too wide for target searching function.

In this paper, three beam-scanning antenna arrays based on two identical monopole slot antennas are shown. Two straight slots are cut at the edge of the finite ground plane of a microstrip structure. The radiating element is a rectangular open slot of total length $0.25\lambda_g$ to achieve a compact design. From the results of radiation characteristics, power-combining characteristics between the two monopole slots are studied and analyzed by varying the separation between the two slots.

Furthermore, three linear arrays of two identical antenna elements with two distinct modes: in-phase or anti-phase (out-of-phase), are shown, and thus an identification of which mode the array will be operating in, depending on the phase difference of the input signals, can be ascertained prior to an array construction. Finally, the two-dimensional beam-scanning characteristics are shown.

2. CONFIGURATIONS OF ANTENNA STRUCTURES

The conventional single open slot antenna geometry with coordinate system is shown in Fig. 1. In this study, the dimensional parameters of the antenna topologies, including the locations of the slot, tuning stub, power divider, and feedline line, are also shown in the figures of the antenna configuration. The tested antennas in our experiment are printed on a circuit board material such as FR-4 substrate ($\varepsilon_r = 4.4$, $\tan\delta = 0.02$, $h = 1.6\,\text{mm}$) and fed by a high-impedance feeding line of width 0.7 mm. The signal is injected into the circuit board via a SMA (Sub-Miniature-A) connector. A monopole slot is cut at the edge of the finite ground plane of a microstrip structure. Its length, $S_L = 20\,\text{mm}$, is approximately a quarter guided wavelength at 2.4 GHz. The ground plane for each of the following cases has a size of $150 \times 100\,\text{mm}^2$. In order to decrease the impedance mismatching condition due to the high impedance of the slot antenna, an open-circuited tuning stub is connected to a 50-Ω microstrip transmission line.

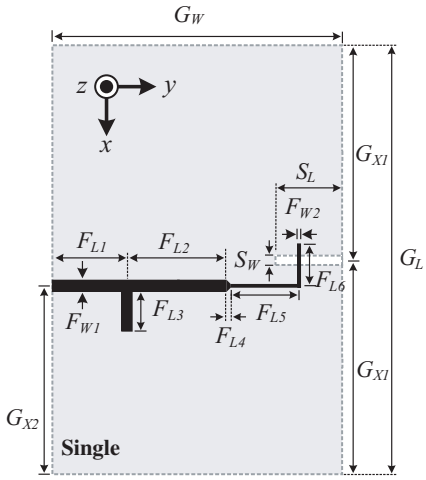

Parameter	(mm)	Parameter	(mm)
G_L	150	F_{L2}	22.15
G_W	100	F_{L3}	12.5
S_L	20	F_{L4}	1.15
S_W	3	F_{L5}	20.35
G_{X1}	75	F_{L6}	12.65
G_{X2}	66.6	F_{W1}	3
F_{L1}	41.7	F_{W2}	0.7

Figure 1. Configuration of a conventional single slot antenna.

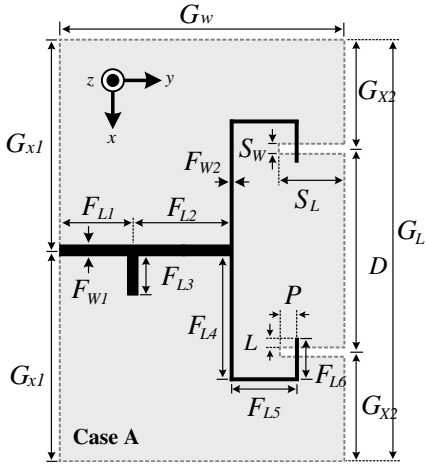

Parameter	(mm)	Parameter	(mm)
G_L	150	F_{L3}	11.2
G_W	100	F_{L4}	38.15
S_L	20	F_{L5}	20
S_W	3	F_{L6}	12.65
G_{X1}	75	F_{W1}	3
G_{X2}	43.75	F_{W2}	0.7
D	62.5	L	2.75
F_{L1}	43	P	5
F_{L2}	22		

Figure 2. Linear array of Case A.

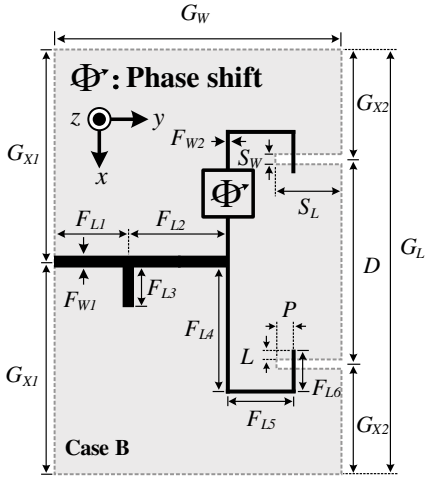

Parameter	(mm)	Parameter	(mm)
G_L	150	F_{L3}	7.6
G_W	100	F_{L4}	38.15
S_L	20	F_{L5}	20
S_W	3	F_{L6}	12.65
G_{X1}	75	F_{W1}	3
G_{X2}	43.75	F_{W2}	0.7
D	62.5	L	2.75
F_{L1}	41.7	P	5
F_{L2}	23.3		

Figure 3. Linear array of Case B.

Figure 2 illustrates a linear array (Case A) of two identical radiating elements with an anti-phase signal injection. Each element is designed to have the same dimensions as the single slot antenna in Fig. 1. A T-junction power divider is used to provide equal power, where each half of the input signal is injected into the input port of two open slot antennas. The feeding ports at the two slot edges are in opposite directions. Two antenna elements are separated by one half

of the free-space wavelength in order to yield desired directivity [18]. It is noted that the phase of the signal at the input port of each slot is equal (in-phase). The second array topology (Case B) is shown in Fig. 3. In order to change the phase difference between the two radiating elements, a phase shifter was designed and embedded into the transmission line between the power divider and one slot element to modulate the phase difference between the two input signals. Fig. 4 shows the simplified schematic diagram of the varactor-tuned phase shifter. The varactor-tuned phase shifter could be designed by using a commercially available CAD tool. Varactor-diode phase shifters are basically analog devices in which the variable reactance is achieved

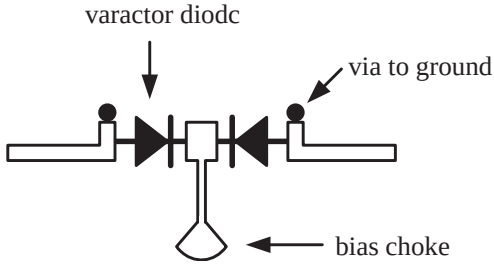

Figure 4. Simplified schematic diagram of the varactor-tuned phase shifter.

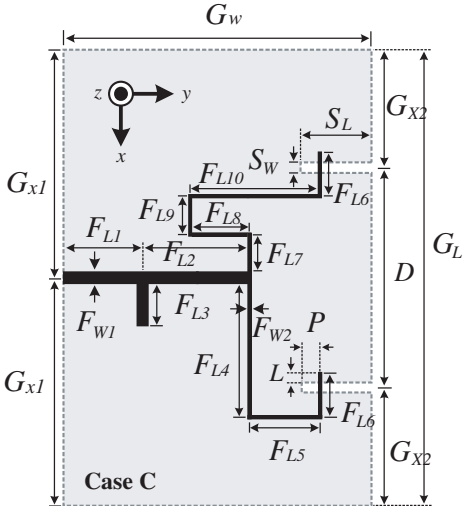

Parameter	(mm)	Parameter	(mm)
G_L	150	F_{L5}	20
G_W	100	F_{L6}	12.65
S_L	20	F_{L7}	12.65
S_W	3	F_{L8}	8.05
G_{X1}	75	F_{L9}	8.7
G_{X2}	43.75	F_{L10}	28.05
D	62.5	F_{W1}	3
F_{L1}	40.6	F_{W2}	0.7
F_{L2}	24.4	L	2.75
F_{L3}	7.2	P	5
F_{L4}	38.15		

Figure 5. Linear array of Case C.

through voltage-tuned capacitance of the diode under the reverse-bias condition. As the bias voltage of this GaAs varactor (M/A-COM MA46410) is varied from 0 V to a large negative value close to its breakdown voltage, V, and the capacitance of the diode decreases from a maximum value to a low value, with a capacitance ratio of 10 : 1. The maximum phase change can be achieved. As expected, the phase progression of the phase shifter varies linearly with bias voltage. Here, the phase difference is set by 180 degree. The arrangement of the feeding network is unchanged. Fig. 5 presents the third array topology (Case C). The feeding ports are arranged in the same direction. The electric lengths of the transmission lines between the feeding port and the node of the divider are equal. Hence, the phase difference between the signals of the two feeding ports is zero. Finally, the separation (D) between two open slots for the array of Case B is varied to observe the power-combining characteristics.

3. RESULTS AND DISCUSSIONS

We consider an array of two identical antennas placed in the xy-plane. The two antennas are fed by the signals with equal magnitude and a phase shift (ξ) of 0 or 180 degree. The example is shown in Fig. 3, where 2 antenna elements are aligned along the x-axis. After calculation, the normalized array factor (NAF) in the xy-plane can be summed up in a closed form:

$$\mathrm{NAF} = \left|\cos\left(\frac{1}{2}\left(kD\cos\phi + \xi\right)\right)\right| \tag{1}$$

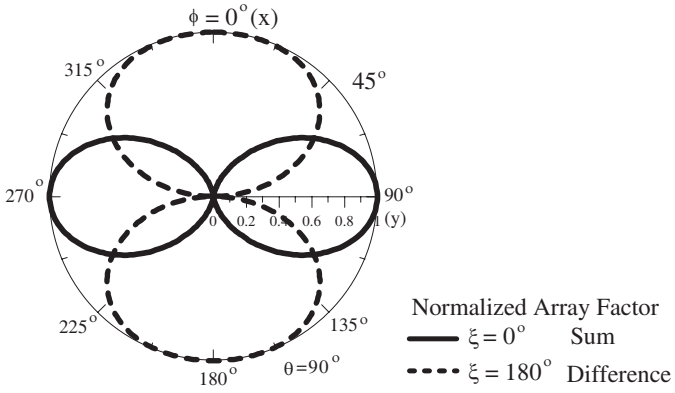

Figure 6. Sketch of the normalized array factor for the two-element array when the phase shift is 0 degree or 180 degree.

It is noted that in Eq. (1) the phase shift (ξ) of the two excitation signals has been taken into consideration, compared to the conventional case. In our study, it is important to derive power-combining radiation pattern, such as the sum pattern. If the phase difference between two injection signals is not properly set, the power leaking from two radiated elements will not successfully combine, and there will be two main beams in the free space, which is called by the difference radiation pattern. Fig. 6 is a sketch of the normalized array factor for the two-element array when the phase shift is 0 degree or 180 degree. The normalized radiation pattern as a function of ϕ depends on the values of the separation D and phase shift ξ. It is shown that a sum pattern can be derived when the phase shift ξ is set by 0 degree. The radiated power of the two antennas is successfully combined. For the case of $\xi = 180$ degree, due to the power divergence, a difference pattern is achieved.

To carry out the Finite Element Method (FEM) investigation, this study uses the High Frequency Structure Simulator (HFSS) commercial software from Ansoft Corporation. Fig. 7 exhibits the comparisons of the simulated and measured reflection coefficients (S_{11}) of the four antenna structures, including the conventional single monopole slot antenna (Single) and three two-element array topologies (Cases A, B, C). As can be observed from the two figures, the resonant frequencies of the four antenna structures are operated around 2.4 GHz,

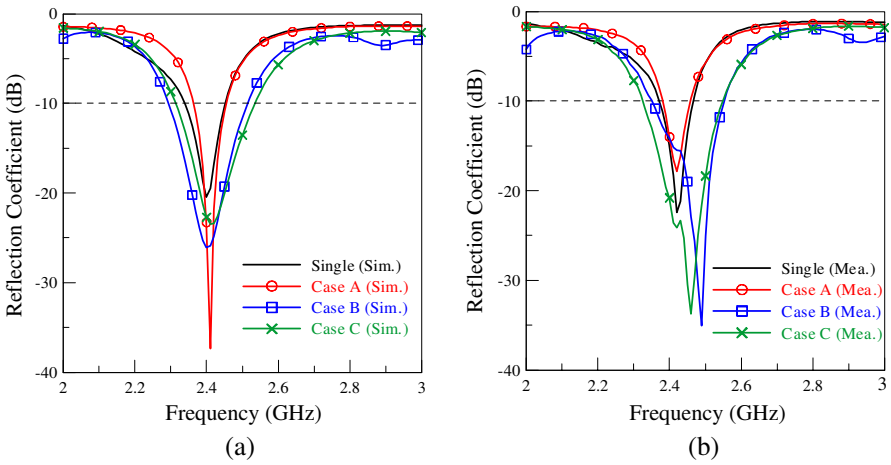

Figure 7. Comparison of the reflection coefficients (S_{11}) of the four antenna structures. (Single, Cases A, B, and C) (a) Simulated. (b) Measured.

as predicted. The simulated and measured results agree well. The slight discrepancy between the simulated and measured results may be attributed to the fabrication misalignment and the physical value of the dielectric constant. In accordance with the measured results, the frequency of the conventional single-slot antenna ranges from 2.38 to 2.46 GHz, and the bandwidth is 80 MHz. The bandwidths of three antenna arrays of Cases A, B, and C are 60 MHz (2.39–2.45 GHz), 190 MHz (2.36–2.55 GHz), and 200 MHz (2.34–2.54 GHz). The bandwidths of the latter two antenna arrays (Cases B and C) are wide than that of the single slot and the array of Case A. Furthermore, the initial resonated frequencies of the latter two arrays also shift down due to enhancement of the impedance bandwidth.

Figure 8 provides the comparison of the simulated radiation patterns of the single monopole slot antenna and the antenna array of Cases A. The simulated surface current densities of the four antennas structures (Single, Cases A, B, and C) at 2.4 GHz are shown in Fig. 9. In Fig. 9(a), for the conventional single monopole antenna, the currents along the edges of the slot are in the opposite directions, so the currents result in the out-of-phase electric fields in free space, and thus the corresponding radiations can be canceled. The useful radiation results from the currents which distribute along the right edges of the ground plane. In Fig. 8, in the xy-plane, due to the feeding network, the left space of the radiation pattern of the conventional single slot antenna is rippled. In the xz-plane, the powers in the transverse directions of $\theta = 0°$ and $\theta = 180°$ are maximum because the current elements flow upward and downward. Hence, the radiation pattern is eight-like. From the results of Fig. 9(b), it can be seen that, for the array of Case A, two in-phase input signals cause the currents at the middle of the left

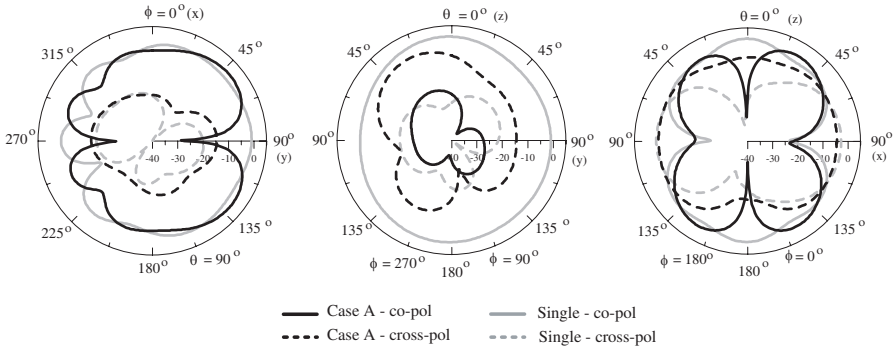

Figure 8. Comparison of the simulated radiation patterns of the single monopole slot antenna and the array of Cases A.

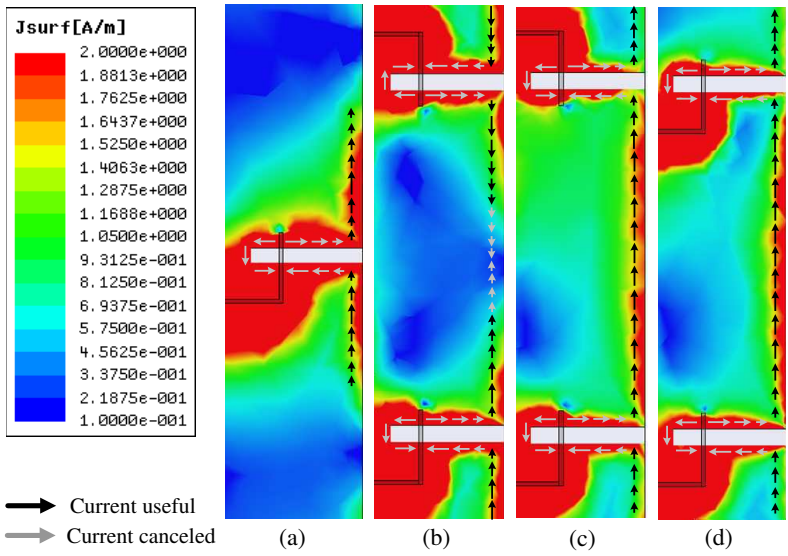

Figure 9. Simulated surface current densities of the four antennas structures at 2.4 GHz. (a) Single. (b) Case A. (c) Case B. (d) Case C.

side of the ground plane canceled and two out-of-phase groups of the currents can not achieve power-combining radiation. In the xy-plane radiation pattern of Fig. 8, it is observed that a different radiation pattern with two maximum powers in the y-direction results from the two out-of-phase current groups because of the anti-symmetrical feeding structure. The out-of-phase currents also contribute to a butterfly-like radiation pattern in the xz-plane. The null points in the y- and z-directions result from the currents, which cancel at the middle of the ground plane. Hence, the two injected signals with equal phase are not suitable for a linear two-element monopole slot antenna array. Meanwhile, in the yz-plane, the power of the array of Case A is much smaller than that of the single monopole slot antenna due to the cancellation of the surface currents.

Figure 10 presents the comparison of the simulated radiation patterns of the two arrays of Cases A and B. As can be observed from the figures, the power-combining characteristics of the Case B array are achieved. In Fig. 9(c), the edge currents distribute in the same direction. Hence, the powers radiating from the two open slots successfully combine, and the main beams reconstruct. Then a sum pattern is derived, instead of a difference pattern. The radiation of the antenna array of Case B is end-fired, as a Yagi antenna. It is noted that the radiation patterns of the single slot antenna and the array of Case

B are similar due to a similar current distribution. The only difference between the patterns is that the y-directional power of the array is stronger than that of the single slot antenna. It may be attributed to the current enhancement at the middle of the edge of the ground plane for the array. Furthermore, as can be observed in the figure, for the Cases B and C, the strong surface current densities, which are at the middle part, radiate more injected power into the space, and the energy stored in the substrate becomes less. This phenomenon may result in a low quality factor and wide bandwidth. It can be explained why the initial resonated frequencies of the Cases B and C shift down in Fig. 7.

Figure 11 shows the comparison of the simulated radiation patterns of the two arrays of Cases A and C. It is shown that the

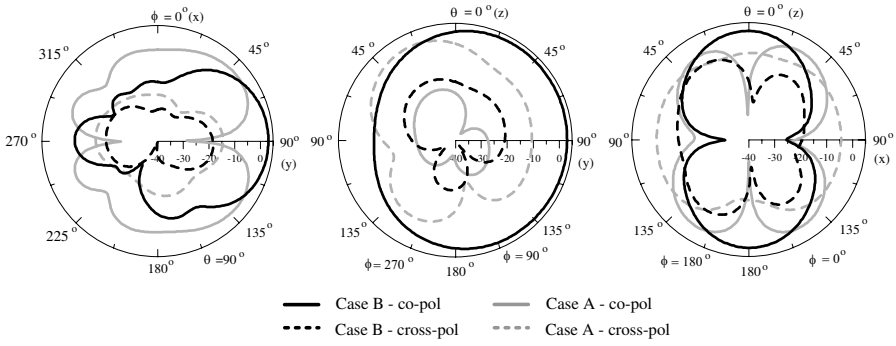

Figure 10. Comparison of the simulated radiation patterns of the antenna arrays of Cases A and B.

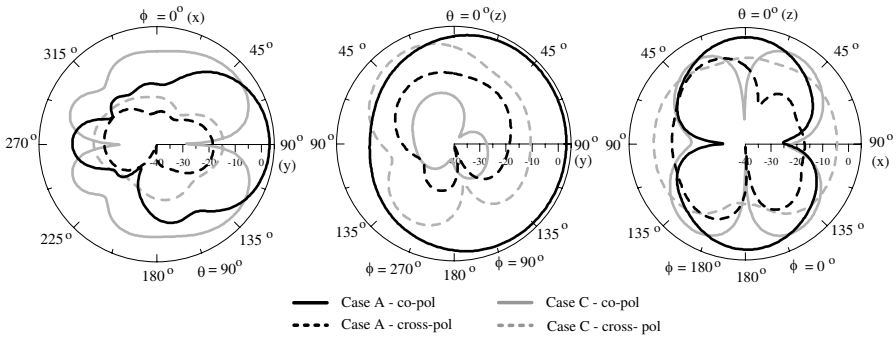

Figure 11. Comparison of the simulated radiation patterns of the antenna arrays of Cases A and C.

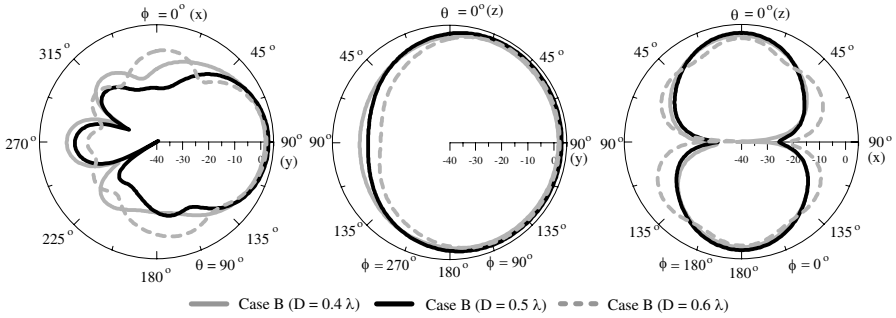

Figure 12. Comparison of the simulated radiation patterns with three different separations (D) between the two open slots.

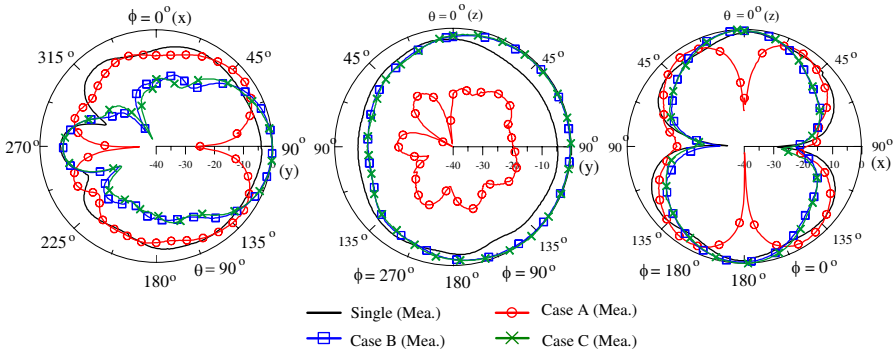

Figure 13. Comparison of the measured radiation patterns of the four antenna structures. (Single, Cases A, B, and C).

good power-combining characteristics of the array of Case C are achieved. It is also seen that the radiation patterns are as similar as those of the array of Case B. Table 1 lists the results of the radiation characteristics for the four antenna structures, including the conventional single slot and the three arrays (Cases A, B, and C). The $+y$- and z-directional power intensities of the latter two arrays (Cases B and C) are approximately double to those of the conventional single-slot antenna and the array of Case A due to the successful power combination in the free space. The 3 dB-beamwidths of the latter two arrays in the xy- and yz-planes become sharp than those of the other two cases (Single and Case A). It is also noted that the front-to-back (F/B) power ratios of the latter two arrays are superior, compared to the first two cases.

Figure 12 shows the comparison of the simulated radiation

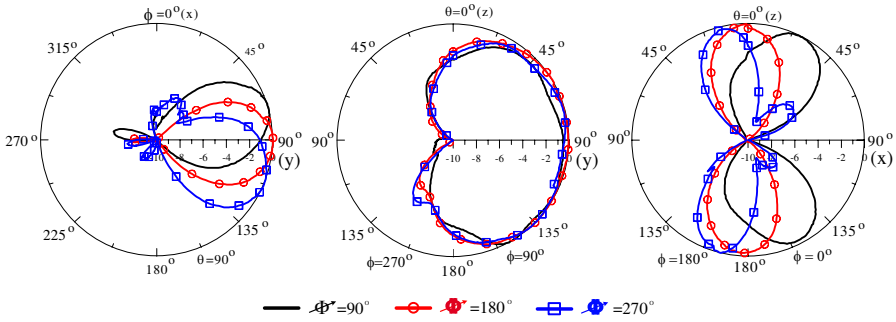

Figure 14. Measured beam-scanning radiation patterns of the array of Case B with different phase difference (90°, 180°, 270°)

Table 1. Radiation characteristics of the four antenna structures.

Parameters \ Case			Single	Case A	Case B	Case C
xy plane	Gain (dB)	$+y$	−0.97	−27.45	3.01	3.11
		$-y$	−4.09	−24.91	−8.66	−7.6
		$+x$	−2.74	−4.48	−19.37	−17
		$-x$	−3.72	−4.6	−12.92	−11.61
		F/B ratio	3.12	−2.54	11.68	10.87
	3 dB beamwidth (degree)		186	N/A	60	64
yz plane	3 dB beamwidth (degree)		286	67	211	194
xz plane	Gain (dB)	$+z$	0.67	−21.93	1.72	1.17
		$-z$	0.08	−31.66	1.57	0.89
		$+x$	−23.33	−21.84	−25.43	−24.64
		$-x$	−24.38	−19.06	−30.85	−31.44
	3 dB beamwidth (degree)		44	N/A	51	54

patterns of the two-element slot antenna array of Case B with respect to three different separations (D) between the two open slots. From the results, it is shown that the beamwidth in every plane decreases effectively when D increases. The power gains in the end-fire direction (the $+y$-direction) for $D = 0.4\lambda$, 0.5λ, and 0.6λ are 1.72 dB, 3.01 dB, and 2.22 dB. Moreover, the power gains in the broadside direction (the $+z$-direction) for $D = 0.4\lambda$, 0.5λ, and 0.6λ are 0.69 dB, 1.72 dB, and −0.29 dB.

Figure 13 illustrates the comparison of the measured radiation patterns of the four antenna structures, including the conventional single slot and the three arrays (Cases A, B, and C). The 3 dB-

beamwidth and gain for different antenna topologies are shown in Table 1. As predicted, the sum patterns in every plane demonstrate good power-combining capability for the arrays of Cases B and C. The maximum power-intensity point is at the end-fire ($+y$-direction) direction of the substrate, where it is at the angle of $\theta = 90^\circ$ and $\phi = 90^\circ$. The measured beam-scanning radiation patterns of the array of Case B are shown in Fig. 14. It is noted that the phase difference of the phase shifter is varied by 90°, 0°, and 270°. It is easily implemented by changing the electric lengths of the transmission lines of the T-junction power divider to achieve the phase difference. The two-dimensional electronically scanning characteristics are observed in the xy- and xz-planes. As can be seen from the figure, the radiation angle of the main beam in the xy-plane is increased from 74° to 113° as the phase difference is increased from 90° to 270°. In the xz-plane, the scanning angles of the dual beams in the $+z$ and $-z$-directions are approximately 43 degrees.

4. CONCLUSION

This work has proposed useful power-combining techniques for the open slot antenna array by comparing four antenna structures, including the conventional single open slot and the three arrays (Case A, B, and C). One technique shown by Case B is to utilize the feeding ports in opposite directions and to inject two out-of-phase signals; on the other hand, the other technique shown by Case C is to utilize the feeding ports in the same direction and to inject two in-phase signals. In Fig. 12, the comparison of the power-combining radiation patterns of the antenna array has been studied by tuning the separation distance. The two-dimensional beam-scanning characteristics are successfully demonstrated for the array of Case B. For antenna designers, the information of this paper will be useful to complete fabrication of the monopole slot antenna array.

ACKNOWLEDGMENT

The research described here was carried out at the RF Circuit and Antenna Laboratory, National University of Tainan, under the Grant: NSC 99-2221-E-024-001 received from the National Science Council, Taiwan. Support for the simulation tools from the National Center for High Performance Computing, Hsinchu, Taiwan is gratefully acknowledged.

REFERENCES

1. Stutzman, W. L. and G. A. Theiele, *Antenna Theory and Design*, 2nd edition, John Wiley, 1998.
2. Humphrey, D. E. J. and V. F. Fusco, "Nonlinear two elements active antenna array stability analysis," *Electron. Lett.*, Vol. 32, No. 9, 788–789, Apr. 1996.
3. Pozar, D. M. and B. Kaufman, "Design considerations for low sidelobe microstrip arrays," *IEEE Trans. Antennas and Propag.*, Vol. 38, No. 8, 1176–1185, Aug. 1990.
4. Liao, P. L. and R. A. York, "A new phase-shifterless beam-scanning technique using arrays of coupled oscillators," *IEEE Trans. Microw. Theory Tech.*, Vol. 41, No. 10, 1810–1815, Oct. 1993.
5. Chew, S. T., T. K. Tong, M. C. Wu, and T. Itoh, "An active phased array with optical input and beam-scanning capability," *IEEE Microw. Guided Wave Lett.*, Vol. 4, No. 10, 347–349, Oct. 1994.
6. Wang, B. and K. M. Huang, "Spatial microwave power combining with anisotropic metamaterials," *Progress In Electromagnetics Research*, Vol. 114, 195–210, 2010.
7. Sirenko, K., V. Pazynin, Y. Sirenko, and H. Baqci, "Compression and radiation of high-power short RF pulses. II. A novel antenna array design with combined compressor/radiator elements," *Progress In Electromagnetics Research*, Vol. 116, 271–296, 2010.
8. Zhao, P. and J. Rahola, "Quarter-wavelength wideband slot antenna for 3–5 GHz mobile applications," *IEEE Antennas Wireless Propag. Lett.*, Vol. 4, 421–424, 2005.
9. Latif, S. I., L. Shafai, and S. K. Sharma, "Bandwidth enhancement and size reduction of microstrip slot antenna," *IEEE Trans. Antennas and Propag.*, Vol. 53, 994–1003, Mar. 2005.
10. Rajgopal, S. K. and S. K. Sharma, "Investigations on ultra-wideband pentagon shape microstrip slot antenna for wireless communications," *IEEE Trans. Antennas and Propag.*, Vol. 57, 1353–1359, May 2009.
11. Chiu, F. H. and K. L. Wong, "Simple folded monopole slot antenna for penta-band clamshell mobile phone application," *IEEE Trans. Antennas and Propag.,* Vol. 57, No. 11, 3680–3684, Nov. 2009.
12. Lai, M. I., T. Y. Wu, J. C. Hsieh, C. H. Wang, and S. K. Jeng, "Compact switched-beam antenna employing a four-element slot antenna array for digital home applications," *IEEE Trans.*

Antennas and Propag., Vol. 56, No. 9, 2929–2936, Sep. 2008.

13. Zhang, F., F.-S. Zhang, C. Lin, G. Zhao, and Y.-C. Jiao, "Design and parameter study of a small size tapered slot antenna," *Journal of Electromagnetic Waves and Applications*, Vol. 23, Nos. 5–6, 655–661, 2009.
14. Zheng, Z.-A., Q.-X. Chu, and T.-G. Huang, "Compact ultra-wideband slot antenna with stepped slots," *Journal of Electromagnetic Waves and Applications*, Vol. 24, Nos. 8–9, 1069–1078, 2010.
15. Su, M., Y.-A. Liu, S.-L. Li, and C.-P. Yu, "A compact open slot antenna for UWB applications with band-notched characteristic," *Journal of Electromagnetic Waves and Applications*, Vol. 24, Nos. 14–15, 2001–2010, 2010.
16. Zhu, X.-F. and D.-L. Su, "A study of a compact microstrip-fed UWB antenna with an open T-Slot," *Progress In Electromagnetics Research Letters*, Vol. 13, 181–189, 2010.
17. Hu, W., Y.-Z. Yin, X. Yang, K. Song, Z.-Y. Liuand, and L.-H. Wen, "A wide open U-Slot antenna with a pair of symmetrical L-strips for WLAN applications," *Progress In Electromagnetics Research Letters*, Vol. 16, 141–149, 2010.
18. Riblet, H. J., "Discussion on 'A current distribution for broadside arrays which optimizes the relationship between beamwidth and side-lobe level'," *Proc. IRE*, 489–492, May 1947.